Polarized sorting of the copper transporter ATP7B in neurons mediated by recognition of a dileucine signal by AP-1

Shweta Jain, Ginny G. Farías, and Juan S. Bonifacino
Cell Biology and Metabolism Program, Eunice Kennedy Shriver National Institute of Child Health and Human Development, National Institutes of Health, Bethesda, MD 20892

ABSTRACT **Neurons are highly polarized cells having distinct somatodendritic and axonal domains. Here we report that polarized sorting of the Cu^{2+} transporter ATP7B and the vesicle-SNARE VAMP4 to the somatodendritic domain of rat hippocampal neurons is mediated by recognition of dileucine-based signals in the cytosolic domains of the proteins by the σ1 subunit of the clathrin adaptor AP-1. Under basal Cu^{2+} conditions, ATP7B was localized to the *trans*-Golgi network (TGN) and the plasma membrane of the soma and dendrites but not the axon. Mutation of a dileucine-based signal in ATP7B or overexpression of a dominant-negative σ1 mutant resulted in nonpolarized distribution of ATP7B between the somatodendritic and axonal domains. Furthermore, addition of high Cu^{2+} concentrations, previously shown to reduce ATP7B incorporation into AP-1–containing clathrin-coated vesicles, caused loss of TGN localization and somatodendritic polarity of ATP7B. These findings support the notion of AP-1 as an effector of polarized sorting in neurons and suggest that altered polarity of ATP7B in polarized cell types might contribute to abnormal copper metabolism in the MEDNIK syndrome, a neurocutaneous disorder caused by mutations in the σ1A subunit isoform of AP-1.**

Monitoring Editor
Judith Klumperman
University Medical Centre
Utrecht

Received: Jul 2, 2014
Revised: Sep 30, 2014
Accepted: Oct 30, 2014

INTRODUCTION

Neurons are highly polarized cells having axonal and somatodendritic domains with distinct protein compositions. The steady-state localization of transmembrane proteins to each of these domains depends on their biosynthetic sorting into axonal and somatodendritic transport carriers, subsequently complemented by selective retention and retrieval mechanisms (Lasiecka and Winckler, 2011; Bonifacino, 2014). Somatodendritic sorting is often mediated by discrete signals contained within the cytosolic tails of the transmembrane proteins (West *et al.*, 1997; Jareb and Banker, 1998; Poyatos *et al.*, 2000; Rivera *et al.*, 2003; Farias *et al.*, 2012; Mattera *et al.*, 2014). A subset of somatodendritic sorting signals fitting the tyrosine-based YXXØ motif (where Y is tyrosine, X is any amino acid, and Ø is a bulky hydrophobic amino acid) has been recently shown to interact with the μ1A subunit of the heterotetrameric adaptor protein 1 (AP-1) complex (Farias *et al.*, 2012; Mattera *et al.*, 2014; Figure 1A), a component of clathrin coats associated with the *trans*-Golgi network (TGN) and recycling endosomes (Robinson, 2004; Traub and Bonifacino, 2013). Mutation of the YXXØ signal or inactivation of AP-1 abrogates somatodendritic sorting of the corresponding proteins, resulting in their nonpolarized distribution in rat hippocampal neurons (Farias *et al.*, 2012; Mattera *et al.*, 2014). This role of AP-1 appears phylogenetically conserved, as mutation of the μ1-subunit orthologue UNC-101 in *Caenorhabditis elegans* abolishes the somatodendritic polarity of various receptors and transporters (Dwyer *et al.*, 2001; Bae *et al.*, 2006; Margeta *et al.*, 2009). AP-1 also binds, via its γ and σ1 subunits, a subset of dileucine-based signals fitting the canonical motif [DE]XXXL[LI] (Janvier *et al.*, 2003; Doray *et al.*, 2007; Mattera 2011), but it remains to be determined whether these interactions also mediate somatodendritic sorting.

This article was published online ahead of print in MBoC in Press (http://www.molbiolcell.org/cgi/doi/10.1091/mbc.E14-07-1177) on November 5, 2014.

Address correspondence to: Juan S. Bonifacino (bonifacinoj@helix.nih.gov).

Abbreviations used: AP-1, adaptor protein 1; BCS, bathocuproine disulfonate; DIV, day in vitro; TGN, *trans*-Golgi network.

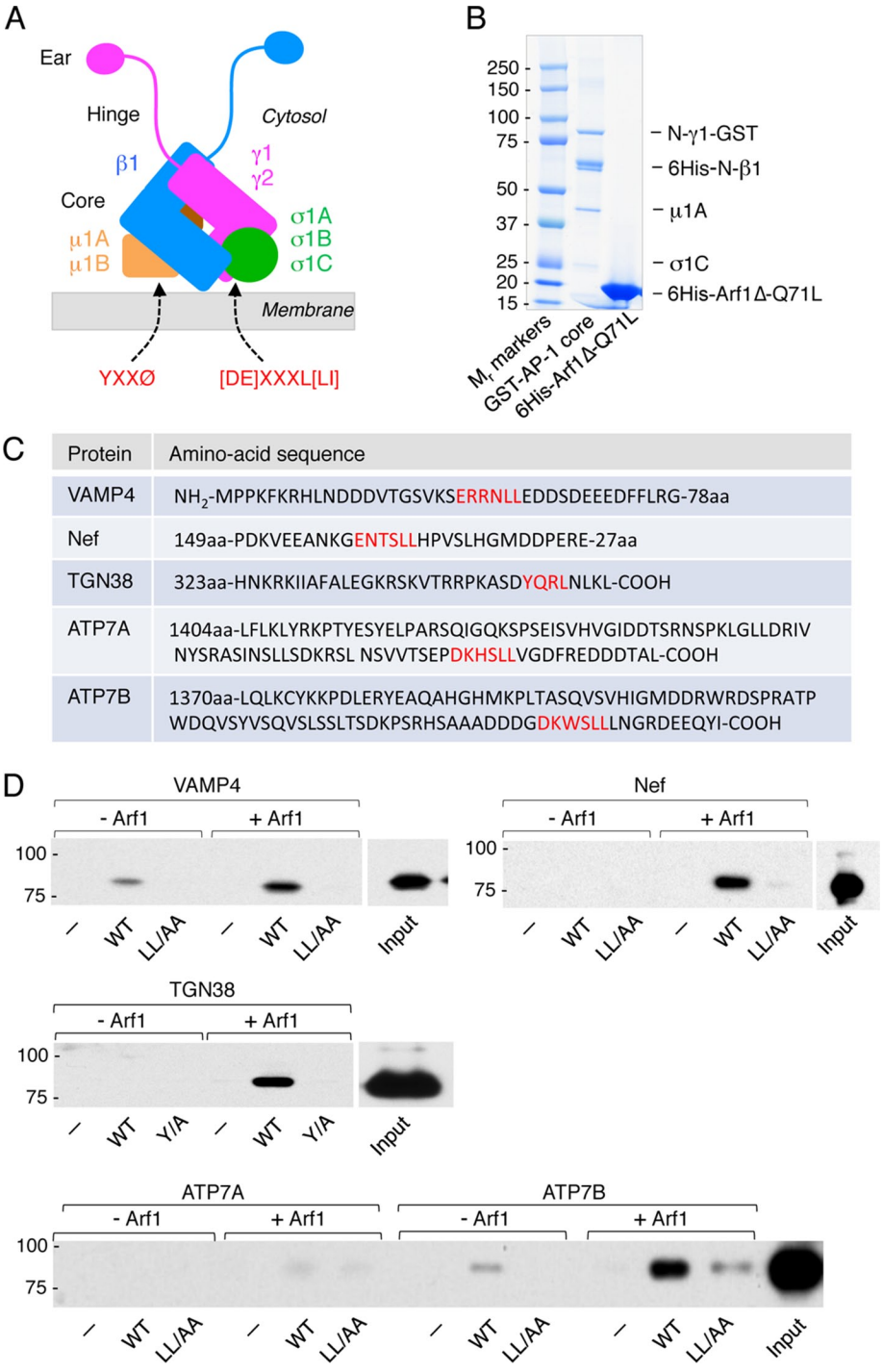

FIGURE 1: Binding of AP-1 to cargo proteins. (A) Schematic representation of the active, membrane-bound conformation of the heterotetrameric (γ-β1-μ1-σ1) AP-1 complex indicating the core, hinge, and ear domains. The γ, μ1, and σ1 subunits occur as two or three isoforms encoded by different genes. YXXØ signals bind to a site on the μ1 subunit, whereas [DE]XXXL[LI] signals bind to a site on the γ-σ1 hemicomplex. (B) SDS–PAGE and Coomassie blue staining of recombinant GST-6His-tagged AP-1 core and 6His-tagged Arf1 used in in vitro pull-down experiments. The AP-1 core used in these experiments was composed of the N-terminal, "trunk" domains of γ1 and β1 and the full-length μ1A and σ1C subunits (Ren *et al.*, 2013). (C) Amino acid sequences of portions of the indicated proteins, with YXXØ and [DE]XXXL[LI] signals highlighted in red. For use in pull-down experiments, an N-terminal maltose-binding protein (MBP) moiety was fused to the mouse VAMP4 cytosolic domain (residues 1–118), the entire HIV-1 Nef (NL4-3 variant), residues 324–353 of the cytosolic tail of rat TGN38, and the C-terminal cytosolic tails of human ATP7A (residues 1405–1500) and ATP7B (residues 1371–1465). (D) Pull down of recombinant GST-His-tagged AP-1 core by MBP-tagged wild-type (WT) or LL/AA (in the [DE]XXXL[LI] signal) or Y/A (in the YXXØ signal) mutant proteins in the absence or presence of GTP-locked Arf1Δ1-16-Q71L. MBP-tagged proteins were immobilized on amylose resin, and bound AP-1 core was analyzed by SDS–PAGE and immunoblotting with antibody to GST. MBP (–) was used as a negative control. The positions of molecular mass markers (in kilodaltons) are indicated on the left.

We decided to examine whether [DE]XXXL[LI]–AP-1 interactions participate in polarized sorting in neurons, with a focus on the mammalian Cu^{2+}-transporting P-type ATPases ATP7A and ATP7B. These transporters are closely related (~60% amino acid identity), multispanning membrane proteins that deliver Cu^{2+} from the cytosol to the lumen of the secretory pathway or the extracellular space (Wang *et al.*, 2011; Polishchuk and Lutsenko, 2013). This transport is required for the loading of copper into cuproenzymes and the efflux of excess copper from the cells. ATP7A is expressed in most tissues, whereas ATP7B has a limited pattern of expression, with highest levels in the liver and lower levels in the brain and kidney. Mutations in ATP7A cause Menkes disease (Online Mendelian Inheritance in Man [OMIM] 309400), an X-linked recessive disorder characterized by general copper deficiency (Kaler, 2013). Mutations in ATP7B, on the other hand, cause Wilson disease (OMIM 277900), an autosomal recessive disorder leading to copper accumulation in the liver and brain (Kaler, 2013). Under basal Cu^{2+} conditions, both transporters exhibit steady-state localization to the TGN (Yamaguchi *et al.*, 1996; Hung *et al.*, 1997). In the presence of high Cu^{2+} levels, however, the transporters redistribute to the plasma membrane and peripheral cytoplasmic vesicles (Petris *et al.*, 1996; La Fontaine *et al.*, 1998; Roelofsen *et al.*, 2000; Guo *et al.*, 2005; Cater *et al.*, 2006; Polishchuk *et al.*, 2014). Subsequent lowering of Cu^{2+} levels causes the transporters to return to the TGN. This retrieval is dependent on dileucine residues fitting the [DE]XXXL[LI] motif in the C-terminal tails of the transporters (Francis *et al.*, 1998; Petris *et al.*, 1998; Cater *et al.*, 2006; Braiterman *et al.*, 2011; Lalioti *et al.*, 2014) and on the AP-1 complex (Holloway *et al.*, 2013). Retrieval to the TGN also correlates with AP-1–dependent packaging of the transporters into clathrin-coated vesicles at low Cu^{2+} levels (Hirst *et al.*, 2012). It remains to be determined, however, whether the [DE]XXXL[LI] motifs in these transporters function through direct interaction with AP-1. Moreover, despite the neuropathological

manifestations of both Menkes disease and Wilson disease, the role of the [DE]XXXL[LI] motifs and the AP-1 adaptor in sorting of the transporters in neurons has not been studied.

In the present study, we tested for interactions of AP-1 with the ATP7A and ATP7B C-terminal tails using a recently developed in vitro pull-down assay involving conformational activation of AP-1 by the Arf1 GTPase (Guo *et al.*, 2013; Ren *et al.*, 2013). We detected weak binding of AP-1 to ATP7A, but strong, [DE]XXXL[LI]-dependent binding of AP-1 to ATP7B. Analysis of the localization of ATP7B in rat hippocampal neurons in primary culture showed that this protein was mainly localized to the TGN, as well as to the plasma membrane of both the soma and dendrites. Remarkably, the protein was largely excluded from the axon, indicating that its distribution in neurons is polarized. Addition of high Cu^{2+} concentrations, previously shown to reduce ATP7B incorporation into AP-1–containing clathrin-coated vesicles (Hirst *et al.*, 2012), caused loss of both TGN localization and somatodendritic polarity of ATP7B. Furthermore, mutation of the [DE]XXXL[LI] motif or overexpression of σ1-subunit mutants incapable of binding [DE]XXXL[LI] signals abrogated the somatodendritic polarity of ATP7B. Similar manipulations also caused loss of somatodendritic polarity of another [DE]XXXL[LI]-containing protein, the vesicle–soluble *N*-ethylmaleimide–sensitive factor attachment protein receptor (v-SNARE) VAMP4. These observations demonstrated that interactions of canonical [DE]XXXL[LI] signals with the σ1 subunit of AP-1 play a general role in protein sorting to the somatodendritic domain. Our findings provide new information relevant to the regulation of brain copper homeostasis under physiological and pathological conditions. In addition, they buttress the proposed explanation for copper metabolism abnormalities in the neurocutaneous disorder MEDNIK syndrome, which is caused by mutation of the σ1A subunit isoform (Montpetit *et al.*, 2008; Martinelli *et al.*, 2013).

RESULTS

Dileucine-dependent binding of the C-terminal tail of ATP7B to AP-1

To search for novel interactions of [DE]XXXL[LI] signals with AP-1 (Figure 1A), we used a recently developed pull-down assay based on the incubation of maltose-binding protein (MBP)–fusion proteins having putative signals with glutathione *S*-transferase (GST)–hexahistidine (6His)–tagged AP-1 core in the presence of the 6His-tagged, GTP-locked form of Arf1 (Arf1Δ-Q71L), all recombinantly produced in *Escherichia coli* (Figure 1B and Supplemental Figure S1; Guo *et al.*, 2013; Ren *et al.*, 2013). Addition of this Arf1 construct induced a conformational activation of the AP-1 core, greatly increasing the sensitivity of the assay (Guo *et al.*, 2013; Ren *et al.*, 2013). The MBP-fusion proteins with bound AP-1 core were collected on amylose beads and analyzed by SDS–PAGE and immunoblotting with antibody to GST. As controls, we showed that the cytosolic domain of the vesicle-SNARE VAMP4 (Peden *et al.*, 2001; Ren *et al.*, 2013) and the Nef protein of HIV-1 (Janvier *et al.*, 2003; Doray *et al.*, 2007; Mattera *et al.*, 2011), both having well-validated [DE]XXXL[LI] signals (Figure 1C), interacted with AP-1 in a dileucine- and Arf1-dependent manner (Figure 1D). Similarly, the cytosolic tail of the TGN protein TGN38, which has a YXXØ signal (Humphrey *et al.*, 1993; Ohno *et al.*, 1995; Figure 1C), also interacted with AP-1 in a tyrosine- and Arf1-dependent manner (Figure 1D). We then used this assay to test for AP-1 binding to the C-terminal cytosolic tails of the Cu^{2+} transporters ATP7A and ATP7B, both having putative [DE]XXXL[LI] signals (DKHSLL and DKWSLL, respectively; Figure 1C). We found that the ATP7A tail bound AP-1 weakly under all the conditions tested (Figure 1D). In contrast, the ATP7B tail exhibited strong, Arf1-dependent interaction with AP-1 (Figure 1D). This interaction was largely abrogated by mutation of Leu-1454 and Leu-1455 within the [DE]XXXL[LI] motif (Figure 1D). On the basis of these results, we focused our subsequent experiments on the role of [DE]XXXL[LI]–AP-1 interactions in neuronal trafficking of ATP7B.

Cu^{2+}-regulated, dileucine-dependent localization of ATP7B to the neuronal TGN

ATP7B is mainly expressed in the liver but has also been detected in select areas of the brain, including the developing CNS (Kuo *et al.*, 1997), the hippocampus (Saito *et al.*, 1999), and the cerebellum (Barnes *et al.*, 2005; see also Allen Brain Atlas, www.brain-map.org/). The neurological and psychiatric symptoms of Wilson disease patients are likely secondary to defective copper metabolism in the liver but could be compounded by primary alterations of copper metabolism in the brain (Wang *et al.*, 2011). The intracellular localization and traffic of ATP7B in neurons, however, have not been previously studied. To address this issue, we expressed green fluorescent protein (GFP)–tagged ATP7B by transfection into rat hippocampal neurons in primary culture. The localization of ATP7B was examined by confocal fluorescence microscopy in comparison to organellar markers. We observed that, under normal culture conditions, ATP7B largely colocalized with the TGN marker TGN38 in the neuronal soma, although some was also present at the plasma membrane (Figure 2A). Addition of the Cu^{2+} chelator bathocuproine disulfonate (BCS) for either 2 h (Figure 2B) or overnight (Supplemental Figure S2) had no effect on this localization. In contrast, incubation with high Cu^{2+} concentrations (200 μM) for 2 h caused redistribution of ATP7B from the TGN to the plasma membrane and peripheral vesicles (Figure 2C). Thus the intracellular localization of ATP7B in neurons is subject to regulation by Cu^{2+} levels, as previously shown in other cell types (Roelofsen *et al.*, 2000; Guo *et al.*, 2005; Cater *et al.*, 2006). Of importance, mutation of the dileucine residues Leu-1454 and Leu-1455 in the [DE]XXXL[LI] motif (Figure 1C) caused a similar redistribution of ATP7B to the cell periphery (Figure 2D), consistent with a function of this motif in determining TGN localization (Francis *et al.*, 1998; Petris *et al.*, 1998; Cater *et al.*, 2006; Braiterman *et al.*, 2011; Lalioti *et al.*, 2014).

Somatodendritic polarity of ATP7B depends on a dileucine motif

Inspection of the neurons expressing GFP-tagged ATP7B using higher gain settings in the confocal microscope revealed that this protein was restricted to the soma and dendrites (marked by MAP2 staining) and largely excluded from the axon (marked by staining of the axon initial segment for ankyrin G) under normal culture conditions (Figure 3A). Mutation of the dileucine residues in the [DE]XXXL[LI] motif resulted in loss of somatodendritic polarity, as evidenced by the appearance of ATP7B in the axons (Figure 3B). Quantification of fluorescence intensities in dendrites and axons from many cells yielded a dendrite/axon "polarity index" of 9.9 ± 2.6 for the normal protein and 1.3 ± 0.4 for the dileucine mutant (Figure 3C). From these experiments, we concluded that the [DE]XXXL[LI] motif mediates not only TGN localization (Figure 2) but also somatodendritic polarity of ATP7B (Figure 3).

Characterization of σ1 subunit mutants for use as dominant-negative constructs

The atomic structure of the AP-1 core in complex with a [DE]XXXL[LI] signal has not yet been solved by x-ray crystallography. However, structural analyses of the unliganded AP-1 core (Heldwein *et al.*, 2004; Ren *et al.*, 2013) and the homologous AP-2 core in complex

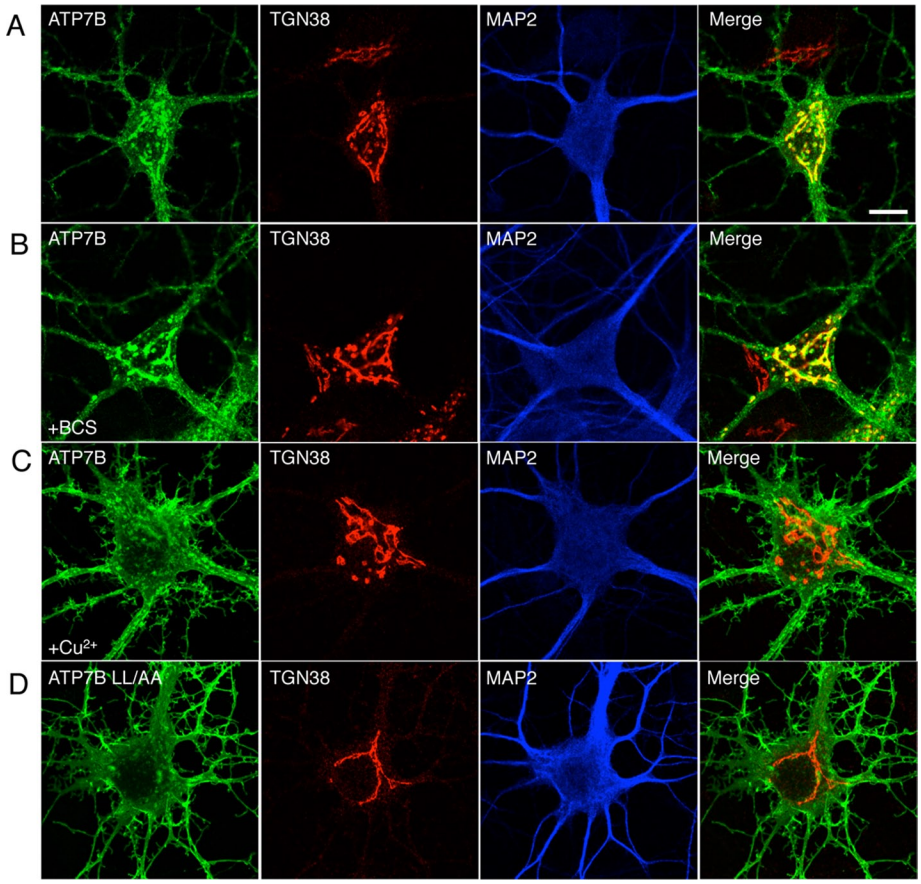

FIGURE 2: A dileucine motif mediates localization of ATP7B to the TGN in neurons. Rat hippocampal neurons in primary culture expressing wild-type (A–C) or LL/AA mutant ATP7B (D), both tagged with GFP, were incubated for 2 h at 37°C with no additions (A, D), 200 μM BCS (B), or 200 μM $CuCl_2$ (C) before fixation and immunostaining for GFP, TGN38 (TGN marker), and MAP2 (somatodendritic marker). Cells were imaged by confocal fluorescence microscopy. Rightmost images are merges of GFP-ATP7B (green) and TGN38 (red). Scale bar, 10 μm.

with a dileucine signal (Kelly *et al.*, 2008; Ren *et al.*, 2014), as well as mutational analyses of [DE]XXXL[LI]-AP-1 interactions (Janvier *et al.*, 2003; Mattera *et al.*, 2011), predict that the [DE]XXXL[LI]-binding site on AP-1 is similar to that on AP-2 (Figure 4A). This predicted binding site is located mainly on the σ1 subunit, with a minor contribution of the γ subunit of AP-1 (Figure 4A; Janvier *et al.*, 2003; Mattera *et al.*, 2011). In mammals, the σ1 subunit occurs as three isoforms, σ1A, σ1B, and σ1C, encoded by different genes (Boehm and Bonifacino, 2001). All three σ1 isoforms bind [DE]XXXL[LI] signals with partly overlapping specificities (Mattera *et al.*, 2011). Yeast-three hybrid analyses showed that mutations of various residues in the putative [DE]XXXL[LI]-binding site on σ1A (i.e., R15S, Y62S, A63W, D92W, and V98S) abrogated the interaction with the [DE]XXXL[LI]-containing VAMP4 cytosolic domain (Figure 4B). We took advantage of this information to devise a dominant-negative approach to interfere with [DE]XXXL[LI]-signal recognition in vivo. The approach consisted of overexpressing a σ1 mutant incapable of binding [DE]XXXL[LI] signals and examining the distribution of [DE]XXXL[LI]-containing proteins in neurons. For this approach to work, the σ1 mutant should be able to assemble into the endogenous AP-1 complex, specifically inactivating the [DE]XXXL[LI]-recognition function of AP-1. We thus tested various mutants in the predicted [DE]XXXL[LI]-binding site on the σ1A, σ1B, and σ1C isoforms tagged with the myc or hemagglutinin (HA) epitopes for assembly into endogenous AP-1. Coprecipitation with the endogenous γ subunit of AP-1 showed that the A63W, V98S, Y62S, and R15S mutants of σ1A were all incorporated into AP-1 as efficiently as the wild-type protein (Figure 4C). In contrast, the I103S, E100Y, and V88D σ1A mutants were not incorporated (Figure 4C), probably because of conformational alterations induced by the mutations. The V98S mutants of σ1B and σ1C were also assembled into AP-1 (Figure 4C). Immunofluorescence microscopy of transfected neurons showed that the wild-type and V98S mutant forms of σ1A, σ1B, and σ1C in neurons all exhibited a similar pattern of localization to the TGN (Figure 4D; see also Supplemental Figure S3). ATP7B also colocalized with σ1B, as well as with the endogenous γ subunit at the TGN (Supplemental Figure S4). The V98S σ1 mutants thus fulfilled the requirements for use in dominant-negative interference experiments.

Interaction with AP-1 is critical for somatodendritic polarity of ATP7B and VAMP4

To determine whether interaction with σ1 is required for somatodendritic sorting of [DE]XXXL[LI]-containing proteins, we coexpressed GFP-tagged ATP7B with wild-type or V98S forms of myc- or HA-tagged σ1A, σ1B, and σ1C in hippocampal neurons. We observed that whereas expression of wild-type σ1A, σ1B, or σ1C had no effect on the somatodendritic polarity of ATP7B, expression of the corresponding V98S mutants resulted in nonpolarized distribution of the transporter (Figure 5, A–D). To generalize these findings, we extended our analyses to VAMP4 (Figure 6, A–E). We observed that VAMP4 also exhibited somatodendritic polarity (Figure 6A), which was lost upon mutation of the dileucine motif (Figure 6B). Similar to ATP7B, VAMP4 somatodendritic polarity was not affected by overexpression of wild-type σ1B (Figure 6C) but was abrogated by overexpression of the V98S σ1B mutant (Figure 6D). In contrast to these findings, overexpression of the V98S σ1B mutant had no effect on the somatodendritic sorting of the YXXØ-containing transferrin receptor (TfR; Figure 7, A–C), consistent with the recognition of the YXXØ signal by μ1 and not σ1 (Ohno *et al.*, 1995). Thus specific recognition of [DE]XXXL[LI] signals by the σ1 subunit of AP-1 mediates sorting of a subset of transmembrane proteins, including ATP7B and VAMP4, to the neuronal somatodendritic domain.

High Cu^{2+} concentration abrogates the somatodendritic polarity of ATP7B

Live-cell imaging of neurons expressing GFP-ATP7B under basal conditions showed very few GFP-ATP7B–containing particles entering the axon, indicating that this protein was excluded from the axon at the level of the soma (Figure 8A and Supplementary Video S1). Incubation with 200 μM Cu^{2+} for 2 h proved deleterious for the morphology of the neurons under the conditions of live-cell imaging. A milder treatment with 100 μM Cu^{2+} for 1 h, however,

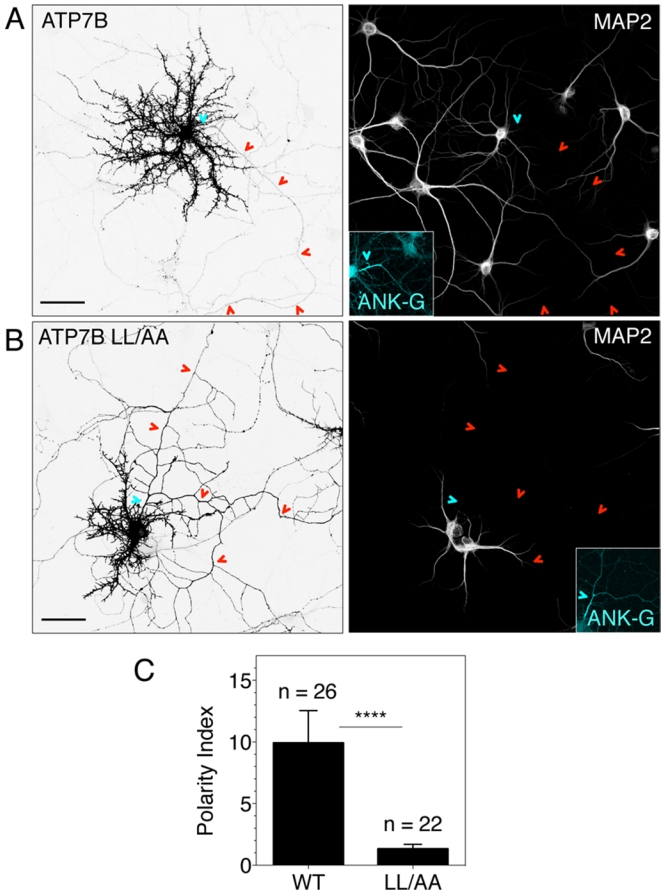

FIGURE 3: Somatodendritic polarity of ATP7B is dependent on a dileucine motif. Rat hippocampal neurons expressing wild-type (A) or LL/AA mutant (B) ATP7B, both tagged with GFP, were fixed and immunostained for GFP, MAP2 (somatodendritic marker), and ankyrin G (ANK-G, marker for the axon initial segment). Cells were imaged by confocal fluorescence microscopy. Negative and positive grayscale images are shown for ATP7B and MAP2, respectively. Cyan arrowheads point to the axon initial segment, and red arrowheads indicate the axon. Scale bar, 50 μm. (C) Quantification of ATP7B polarity. The ratio of fluorescence intensities in dendrites and axons (i.e., polarity index) for wild-type (WT) and LL/AA mutant ATP7B was calculated from the indicated number (*n*) of cells. Values are the mean ± SD. ****$p < 0.0001$.

preserved the morphology of the neurons and revealed movement of a large number of GFP-ATP7B–containing particles from the soma into the axon (Figure 8A and Supplementary Video S1). Quantification of fluorescence intensities in many cells yielded a dendrite/axon polarity index of 8.7 ± 1.8 under basal conditions and 2.5 ± 0.7 upon treatment with 100 μM Cu^{2+} (Figure 8B). Kymographic analysis of the live-cell imaging data showed increased numbers of both anterograde (lines with negative slopes) and retrograde (positive slopes) carriers, as well as stationary foci (vertical lines), in the axons of neurons treated with 100 μM Cu^{2+} (Figure 8C). A recent study showed that elevated Cu^{2+} levels cause movement of ATP7B from the TGN to late endosomes and lysosomes in a hepatoma cell line (Polishchuk *et al.*, 2014). Indeed, we observed that many of the GFP-ATP7B–containing particles that moved into the axon upon treatment with 100 μM Cu^{2+} also contained the late endosomal/lysosomal marker Lamp-1-RFP (Figure 8D). From these experiments, we concluded that elevated Cu^{2+} levels interfere with AP-1–dependent TGN/somatodendritic localization of ATP7B, resulting in its transport to late endosomes or lysosomes capable of moving into the axon.

DISCUSSION

The results presented here demonstrate that interactions of [DE]XXXL[LI]-type dileucine signals with the σ1 subunit of AP-1 underlie the sorting of a subset of transmembrane proteins (e.g., ATP7B, VAMP4) to the somatodendritic domain of neurons. Together with the previous demonstration that interactions of YXXØ-type signals with the μ1A subunit of AP-1 mediate somatodendritic sorting of other transmembrane proteins (Farias *et al.*, 2012; Mattera *et al.*, 2014), our findings support a general role for AP-1 in polarized sorting in neurons. Disruption of signal–AP-1 interactions results in nonpolarized distribution of the proteins to both dendrites and axons, indicating that these interactions normally function to exclude somatodendritic proteins from the axon. The exact mechanism by which AP-1 performs this exclusion remains to be elucidated. In the case of ATP7B, somatodendritic sorting correlates with concentration of this protein at the TGN, suggesting that axonal exclusion requires AP-1–dependent localization or retrieval to the TGN. Presumably AP-1 acts by segregating somatodendritic proteins away from TGN or recycling endosomal sites that give rise to axonal carriers.

In addition to shedding light on a general mechanism of polarized sorting, our findings reveal new aspects of the trafficking of a physiologically important protein, ATP7B. Previous studies of ATP7B traffic had been done in liver and epithelial cells but not in neurons. We find that ATP7B predominantly localizes to the TGN under basal conditions. We also observe localization of ATP7B to the plasma membrane of the soma and dendrites but not the axon. This distribution is consistent with cycling between the TGN and the somatodendritic plasma membrane under low Cu^{2+} levels. The somatodendritic restriction of ATP7B likely ensures efficient copper loading of cuproenzymes, such as peptidylglycine α-amidating monooxygenase (PAM; also an AP-1–interacting cargo; Bonnemaison *et al.*, 2014), in the perikaryon, as well as protection from copper toxicity in the axon, as suggested by the deleterious effects of some missense mutations of the related ATP7A in distal motor neuropathies (Kennerson *et al.*, 2010; Yi *et al.*, 2012). High Cu^{2+} levels, however, cause ATP7B redistribution from the TGN to cytoplasmic vesicles that are capable of moving into the axon. Some of these vesicles also contain Lamp-1, identifying them as late endosomal/lysosomal compartments. These observations are in line with the reported high-Cu^{2+}–induced relocalization of ATP7B to late endosomes and lysosomes and eventually to the bile canalicular surface in a hepatoma cell line (Polishchuk *et al.*, 2014) and with the ability of lysosomes to undergo axonal transport (Mar *et al.*, 2014; Otero *et al.*, 2014). It thus appears that the mechanisms that regulate transport of ATP7B are conserved in different polarized cell types. Because somatodendritic sorting of ATP7B depends on [DE]XXXL[LI]–AP-1 interactions, it would now be of interest to study whether these interactions also mediate polarized sorting of ATP7B in hepatocytes, where this protein is most highly expressed.

It remains to be determined to what extent the neurological manifestations of Wilson disease are an indirect consequence of copper metabolism dysregulation in the liver or a direct result from its alteration in the brain (Emre *et al.*, 2001; Schumacher *et al.*, 2001). In any event, our findings provide important new information on the neuronal trafficking of a key regulator of iron metabolism that may be applicable to its trafficking in other polarized cell types, including hepatocytes. Our findings might also contribute to explaining the pathogenesis of the genetic disease MEDNIK syndrome, which is

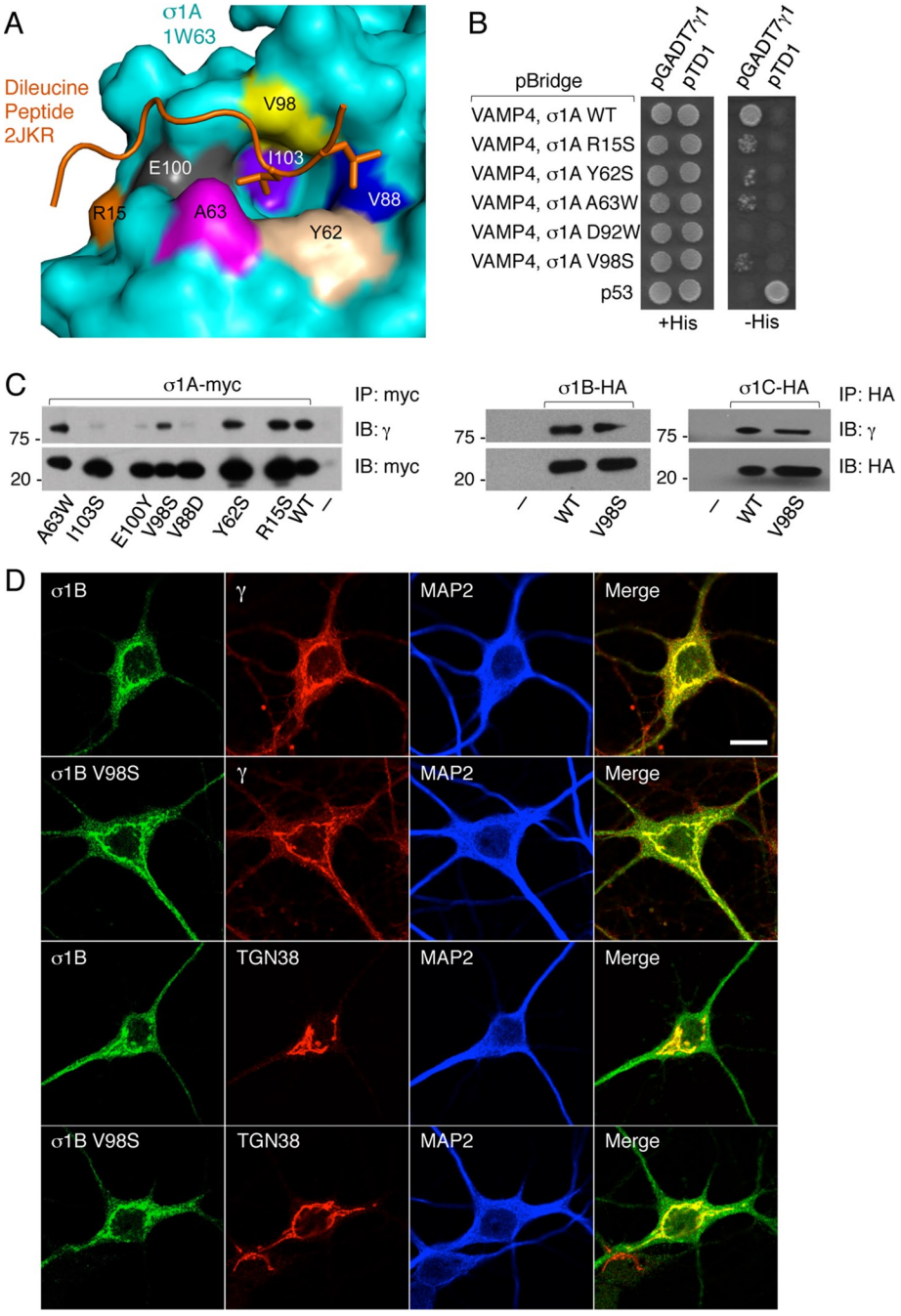

FIGURE 4: Mutational analysis of σ1 residues involved in recognition of dileucine motifs. (A) Surface representation of the predicted binding site for dileucine signals on the γ-σ1A hemicomplex based on the crystal structures of the unliganded AP-1 core (Heldwein *et al.*, 2004; Ren *et al.*, 2013) and AP-2 in complex with the dileucine signal from CD4 (Kelly *et al.*, 2008) and previous biochemical analyses (Mattera *et al.*, 2011). Protein Data Bank accession codes are indicated. Residues targeted for mutagenesis are highlighted. (B) Yeast three-hybrid (Y3H) analysis of the interaction of the cytosolic domain (residues 1–118) of VAMP4 with wild-type (WT) σ1A and the indicated σ1A mutants. Growth of transformants on plates lacking histidine (–His) indicates interactions. (C) Incorporation of transgenic σ1 constructs into the endogenous AP-1 complex. HeLa cells were transfected with plasmids encoding the indicated WT or mutant σ1A, σ1B, or σ1C isoforms tagged with the myc or HA epitopes. Cell extracts were subjected to immunoprecipitation (IP) with antibody to the myc or HA epitopes, followed by immunoblotting (IB) with antibody to the endogenous γ subunit of AP-1 or to the myc or HA epitopes, as indicated. Untransfected HeLa cells were used as a negative control (–). (D) Confocal immunofluorescence microscopy of rat hippocampal neurons expressing transgenic wild-type or V98S-mutant σ1B tagged with the HA epitope. Cells were immunostained for HA (transgenic σ1B subunit; green), for the γ subunit of AP-1 or TGN38 (red), and for MAP2 (blue). Rightmost images are merges of the green (σ1B-HA) and red (γ-adaptin or TGN38) channels. Scale bar, 10 μm.

caused by mutations in the AP1S1 gene encoding the σ1A subunit of AP-1 (Montpetit *et al.*, 2008). MEDNIK is an acronym for the main symptoms of this disease: mental retardation, enteropathy, deafness, neuropathy, ichthyosis, and keratodermia. Of note, these manifestations all involve organs with a core component of polarized cells, including neurons and epithelial cells. Given the function of AP-1 in sorting to the somatodendritic domain of neurons (Farias *et al.*, 2012; Mattera *et al.*, 2014) and the basolateral domain of epithelial cells (Folsch *et al.*, 1999; Carvajal-Gonzalez *et al.*, 2012; Gravotta *et al.*, 2012), it is reasonable to hypothesize that defects in polarized sorting of specific cargo proteins might contribute to the symptoms of MEDNIK syndrome. Why does a defect in only one σ1 subunit isoform, σ1A, cause this condition? The σ1A, σ1B, and σ1C isoforms recognize overlapping but distinct sets of [DE]XXXL[LI] signals (Mattera *et al.*, 2011). It is thus likely that MEDNIK syndrome results from missorting of a σ1A-specific cargo in cells that otherwise express σ1B and σ1C. Alternatively, each σ1 isoform could be expressed in a distinct set of cells, such that loss of σ1A would cause a general failure of AP-1–dependent sorting in the corresponding cell population.

MEDNIK patients have been recently reported to have copper metabolism defects characteristic of both Menkes and Wilson diseases, pointing to ATP7A and ATP7B as likely candidates for missorting in this disease (Martinelli *et al.*, 2013). Indeed, in fibroblasts from MEDNIK patients, ATP7A is not localized to the TGN but to peripheral structures irrespective of Cu^{2+} levels (Martinelli *et al.*, 2013). We did detect specific interaction of the ATP7A tail with the AP-1 core (Figure 1D), but this interaction was too weak for detailed characterization. The weakness of this interaction could be explained by the fact that the AP-1 core construct used in our studies had σ1C instead of σ1A. Although interaction of this core construct with ATP7B was stronger, it is possible that interaction with a σ1A-containing core could have been even stronger. Our studies suggest that in addition to failure to localize to the TGN at low Cu^{2+} levels, altered polarity of ATP7B (and perhaps also ATP7A) in polarized cell types might underlie some of the copper metabolism defects in MEDNIK syndrome. Further studies on the signal-recognition preference and cell-specific expression of the different σ1 subunit isoforms should help elucidate the mechanistic basis for the copper metabolism defects and other symptoms in MEDNIK syndrome.

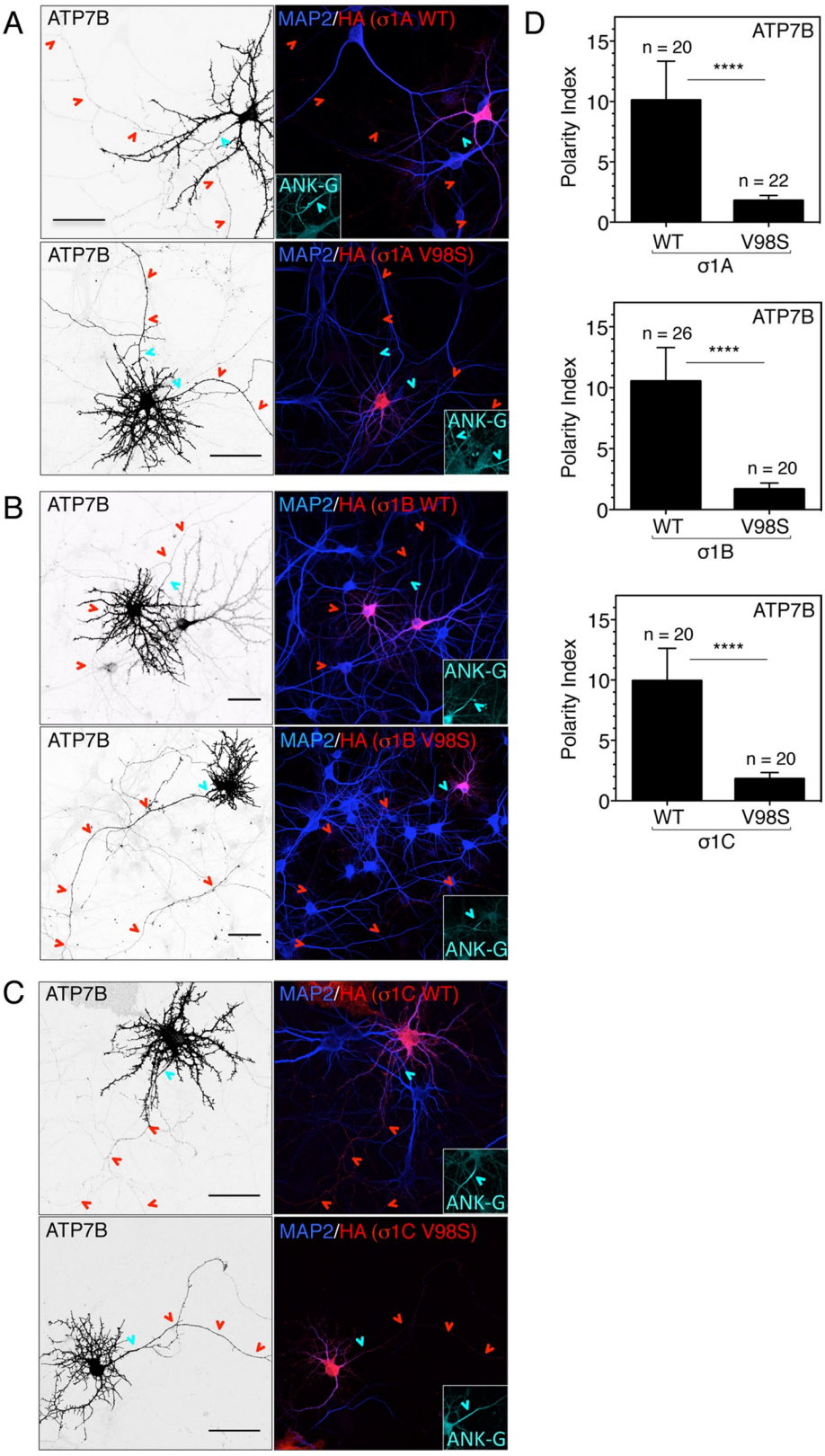

FIGURE 5: Binding of a dileucine motif to the σ1 subunit of AP-1 is required for somatodendritic sorting of ATP7B. (A–C) Rat hippocampal neurons coexpressing GFP-tagged ATP7B with (A) myc-tagged WT or V98S-mutant σ1A, (B) HA-tagged WT, or (C) V98S-mutant σ1B, HA-tagged WT, or V98S-mutant σ1C were fixed and immunostained for GFP (negative grayscale images, left), the HA epitope, or the myc epitope (red), MAP2 (blue), and ankyrin G (ANK-G; cyan) as indicated. Cells were imaged by confocal fluorescence microscopy. Cyan arrowheads point to the axon initial segment, and red arrowheads mark the axon. Scale bar, 50 μm. (D) Quantification of the dendrite/axon polarity index for ATP7B when coexpressed with WT or V98S-mutant σ1B, σ1A, or σ1C, as indicated. Values are the mean ± SD from the indicated number (*n*) of cells. ****$p < 0.0001$.

MATERIALS AND METHODS

DNA constructs and mutagenesis

The cDNA encoding human σ1A tagged at the C-terminus with three copies of the myc epitope (σ1A-myc) was cloned into pcDNA3.1 (Hygro+; Life Technologies, Grand Island, NY), and those encoding human σ1B or σ1C tagged at the C-terminus with three copies of the HA epitope (σ1B-HA, σ1C-HA) were cloned into pCI-neo (Promega, Madison, WI). The cDNAs encoding the full-length or cytosolic portion of wild-type and mutant cargo proteins were cloned into a modified pHis2 vector encoding MBP (Ren *et al.*, 2013). Plasmids encoding the recombinant AP-1 core, Arf1Δ1-16-Q71L (referred to as His Arf1Δ-Q71L), and VAMP4-GFP have been described previously (Tran *et al.*, 2007; Guo *et al.*, 2013; Ren *et al.*, 2013). Lamp-1-RFP, plasmid #1817, was obtained from Addgene (submitted by W. Mothes, Yale University School of Medicine, New Haven, CT). Plasmids encoding GFP-ATP7B and TfR-mCherry were gifts from S. Lutsenko (Johns Hopkins University, Baltimore, MD) and J. Lippincott-Schwartz (National Institutes of Health, Bethesda, MD), respectively. Mutagenesis was performed using the QuikChange kit (Agilent, Santa Clara, CA).

Antibodies and other reagents

The antibodies used in this study and their sources are as follows: rabbit anti-MAP2 (Santa Cruz Biotechnology, Dallas, TX); goat anti–ankyrin G (Santa Cruz Biotechnology); chicken anti-GFP (Invitrogen, Carlsbad, CA); mouse anti-TGN38 (Thermo Scientific, Rockford, IL); mouse anti–γ-adaptin (BD Biosciences, San Diego, CA); mouse anti-HA (Covance, Dedham, MA); chicken anti-HA (Millipore, Billerica, MA); chicken anti-MAP2 (Abcam, Cambridge, MA); and mouse anti–pan-neurofascin (external epitope, Clone A12/18; University of California, Davis/National Institutes of Health NeuroMab Facility, Bethesda, MD). Rabbit anti-HA and rabbit anti-myc were gifts from A. Sharma (National Institutes of Health). The antibody to p230 was a gift from M. Krieger (MIT, Cambridge, MA). Rabbit anti-GST antiserum and mouse anti-myc clone 9E10 have been described before (Dell'Angelica *et al.*, 1998; Mattera *et al.*, 2011). Mix-n-stain-CF640R (Biotium, Hayward, CA) was used to label the antibody to neurofascin.

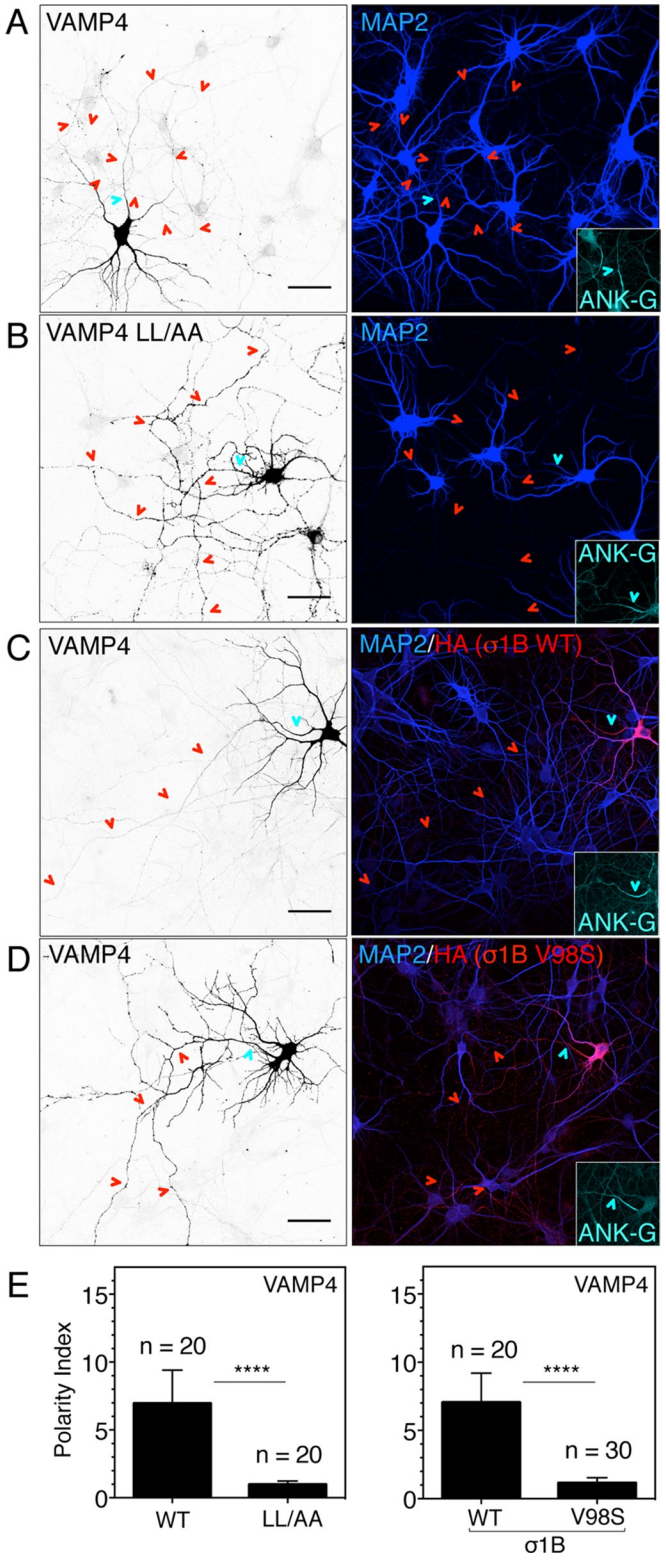

FIGURE 6: Somatodendritic polarity of VAMP4 is dependent on a dileucine motif and its binding to the σ1 subunit of AP-1. (A, B) Rat hippocampal neurons expressing WT (A) or LL/AA mutant (B) VAMP4, both tagged with GFP, were fixed and immunostained for GFP (negative grayscale images, left), MAP2 (blue), and ankyrin G (ANK-G) (cyan). (C, D) Rat hippocampal neurons coexpressing VAMP4-GFP with HA-tagged WT (C) or V98S-mutant σ1B (D) were fixed and immunostained for GFP (negative grayscale images, left), the HA epitope (red), MAP2 (blue), and ankyrin G (ANK-G) (cyan), as indicated. Cyan arrowheads point to the axon initial segment, and red arrowheads mark the axon. Scale bar, 50 μm (E) Quantification of VAMP4 polarity. The ratio of fluorescence intensities in dendrites and axons (i.e., polarity index) for WT and LL/AA mutant VAMP4, and of VAMP4 when coexpressed with WT or V98S-mutant σ1B, was calculated. Values are the mean ± SD from the indicated number (*n*) of cells. **** $p < 0.0001$.

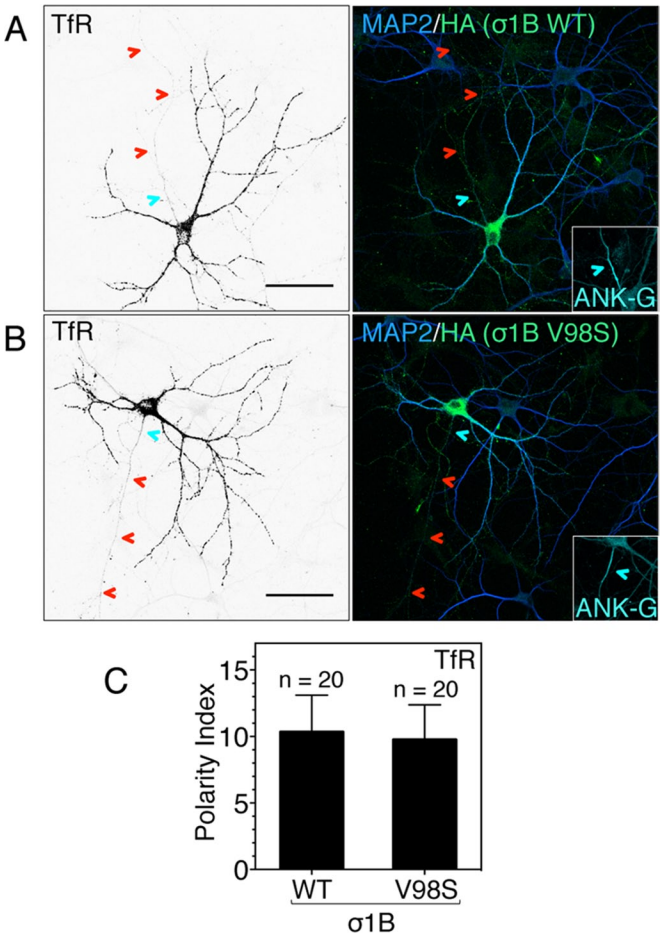

FIGURE 7: Somatodendritic polarity of TfR is independent of the [DE[XXXL[LI]-binding function of σ1. (A, B) Rat hippocampal neurons coexpressing TfR-mCherry (negative grayscale images, left) with HA-tagged WT (A) or V98S-mutant σ1B (B) were fixed and immunostained with antibody to the HA epitope (green), MAP2 (somatodendritic marker; blue), and ankyrin G (ANK-G, marker for the axon initial segment; cyan) as indicated. Cells were imaged by confocal fluorescence microscopy. Cyan arrowheads point to the axon initial segment, and red arrowheads mark the axon. Scale bar, 50 μm (C) Quantification of the dendrite/axon polarity index for TfR-mCherry when coexpressed with WT or V98S-mutant σ1B. Values are the mean ± SD from the indicated number (*n*) of cells.

Recombinant protein purification

MBP-ATP7A, -ATP7B, -VAMP4, -Nef, and -TGN38 fusion proteins, Arf1Δ1-16-Q71L, and AP-1 core were purified from bacterial lysates using nickel-nitriloacetic acid (Qiagen, Valencia, CA), followed by gel filtration (AKTA; GE Healthcare, Piscataway, NJ; Guo *et al.*, 2013; Ren *et al.*, 2013). In the case of the AP-1 core, affinity purification was performed using glutathione–Sepharose 4B (GE Healthcare) before gel filtration. All purified proteins were snap frozen using liquid nitrogen and stored at −80°C.

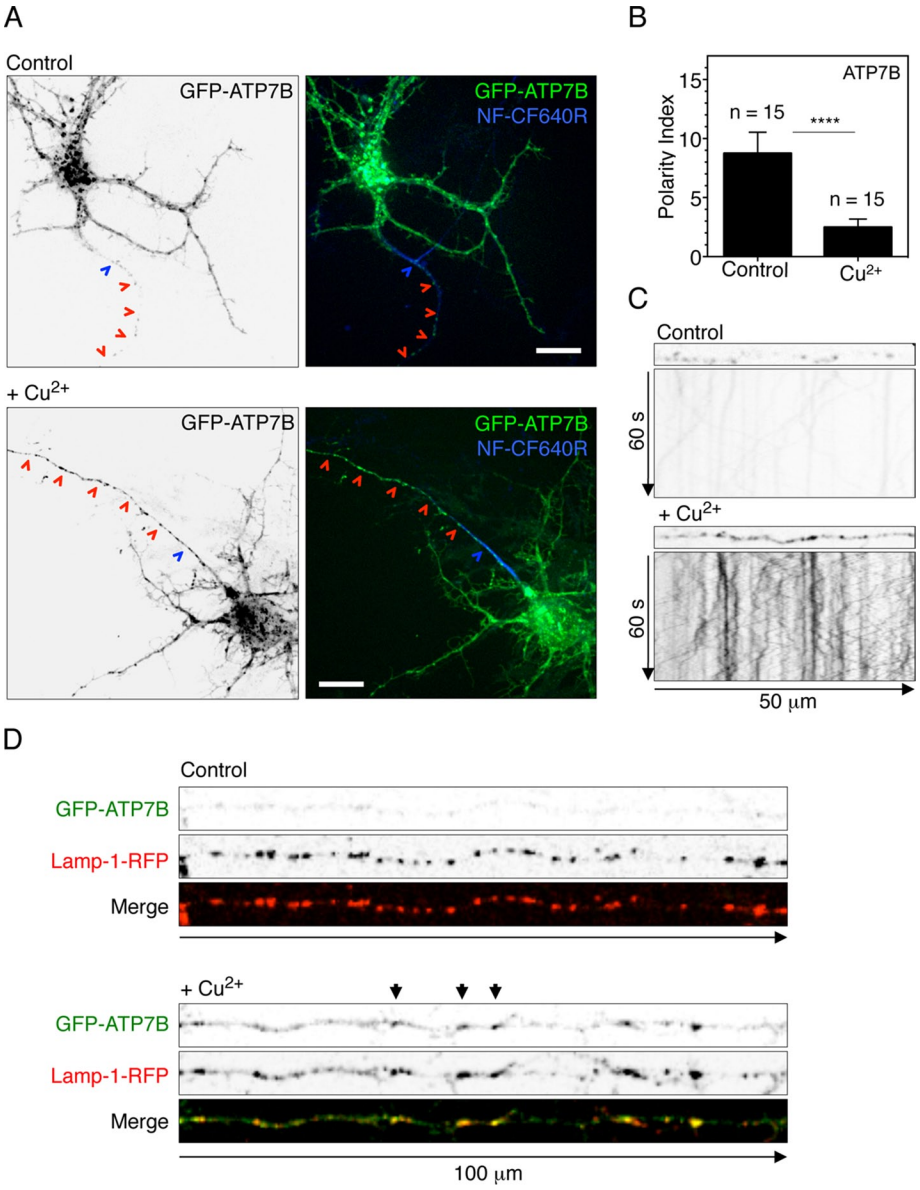

FIGURE 8: High Cu^{2+} concentration redistributes ATP7B to late endosomes or lysosomes that move along the axon in live hippocampal neurons. (A) Negative grayscale (left) and dual-color images (right) of live DIV8 neurons expressing GFP-ATP7B (grayscale and green) and stained for the AIS marker NF-CF640R (blue, right) under control conditions (top) or exposed to 100 μM $CuSO_4$ for 1 h (bottom). Red arrowheads indicate the axon. Blue arrowheads point to the axon initial segment. Scale bar, 20 μm. See also Supplemental Video S1. (B) Quantification of ATP7B polarity in control neurons or neurons exposed to 100 μM $CuSO_4$ for 1 h. Values are the mean ± SD from the indicated number (*n*) of cells. ****$p < 0.0001$. (C) Axon from control neuron (top) and from neuron exposed to $CuSO_4$ (bottom) corresponding to neurons in A and Supplemental Video S1. Kymographs represent the movement of particles containing GFP-ATP7B in 50 μm of axon length from control or Cu^{2+}-treated neurons during 60 s of recording. Axons are orientated so anterograde transport occurs from left to right (negative slopes) and retrograde transport from right to left (positive slopes). (D) Neurons at DIV10 cotransfected with plasmids encoding GFP-ATP7B (negative grayscale and green in merge) and Lamp-1-RFP (negative grayscale and red in merge) were treated with 100 μM $CuSO_4$ for 1 h and compared with control neurons. Notice the presence of late endosomes or lysosomes labeled with Lamp-1-RFP in the axons under both conditions (red). High Cu^{2+} conditions increase the presence of ATP7B in axonal late endosomes or lysosomes, as indicated by arrowheads.

Immunoprecipitation and immunoblotting

The expression and assembly of dominant-negative σ1 mutants tagged with myc or HA was tested by transient transfection in HeLa cells, followed by immunoprecipitation-immunoblotting as previously described (Guo *et al.*, 2013; Mattera *et al.*, 2014).

Yeast three-hybrid analysis

Yeast three-hybrid analysis was performed as previously described (Mattera *et al.*, 2011). The cytosolic domain of VAMP4 (residues 1–118) and the σ1A subunit of AP-1 were cloned in MCS1 and MCS2, respectively, of the same pBridge vector. The plasmids encoding p53, γ1, and SV40 T-Ag were described earlier (Mattera *et al.*, 2011).

Pull-down assay

Interaction of cargo proteins with the AP-1 core in the absence or presence of Arf1Δ1-16-Q71L was analyzed using a previously described pull-down assay (Guo *et al.*, 2013; Ren *et al.*, 2013). In brief, MBP-tagged cargo protein (20 μg) immobilized on amylose resin (New England Biolabs, Beverly, MA) was incubated with 0.05 μM AP-1 core precleared on amylose resin in the absence or presence of 10 μM Arf1Δ1-16-Q71L and 1 mM GTP. The pull down was analyzed by SDS–PAGE, followed by immunoblotting.

Cell culture and transfection

Primary rat hippocampal neurons were prepared as previously described (Kaech and Banker 2006; Farias *et al.*, 2012). Transfections of DNA constructs were performed at day in vitro 3 (DIV3) using Lipofectamine 2000 (Invitrogen), and the transfected neurons were analyzed at DIV10. HeLa cells were maintained in DMEM supplemented with 10% fetal bovine serum, glutamine, and penicillin/streptomycin. Transfections of DNA constructs into HeLa cells were done using Lipofectamine 2000.

Immunostaining, confocal microscopy, and image analysis

Immunostaining and immunofluorescence imaging of transfected hippocampal neurons were performed as previously described (Farias *et al.*, 2012; Mattera *et al.*, 2014). Fluorescence images were acquired using a confocal Zeiss LSM 710 microscope fitted with 40×/1.3 numerical aperture (NA) or 63×/1.4 NA objectives. Analysis of the fluorescence images was done using ImageJ (National Institutes of Health, Bethesda, MD). The polarity index was calculated as previously described (Farias *et al.*, 2012; Mattera *et al.*, 2014). Values are represented as the mean ± SD in all the figures. The statistical analysis was done with a nonparametric *t* test using Prism (GraphPad Software, La Jolla, CA).

Live-cell imaging and kymographic analysis

Hippocampal neurons were transfected on DIV4 with a plasmid encoding GFP-ATP7B. At DIV8, neurons were immunostained with CF640R-conjugated antibody to neurofascin for 30 min at 37°C to identify the axon. Then control neurons and neurons treated with 100 μM $CuSO_4$ for 1 h were imaged on a spinning-disk confocal microscope (Marianas; Intelligent Imaging, Denver, CO) fitted with a 63×/1.4 NA objective. Digital images were acquired with an electron-multiplying charge-coupled device camera (Evolve; Photometrics, Tucson, AZ). For dual-color videos, GFP-ATP7B and NF-CF640R channels were sequentially exposed for 200 and 100 ms, respectively. Neurons were recorded every 500 ms for 60 s. To analyze the movement of vesicles containing GFP-ATP7B, kymographs were generated using ImageJ, version 1.44o. Lines (20 pixels wide, 50 μm long) were traced in the axon and straightened. This was followed by reslicing stacks and construction of *Z*-projections. Tracks were orientated so that anterograde movement occurred from left to right in 60 s of recording.

ACKNOWLEDGMENTS

We thank X. Zhu and N. Tsai for expert technical assistance, X. Ren for help with Figure 4A, S. Lutsenko, M. Krieger, W. Mothes, A. Sharma, and J. Lippincott-Schwartz for kind gifts of reagents, and R. Mattera and S. Kaler for helpful discussions and critical review of the manuscript. This work was funded by the Intramural Program of the National Institute of Child Health and Human Development, National Institutes of Health (ZIA HD001607-22).

REFERENCES

Bae YK, Qin H, Knobel KM, Hu J, Rosenbaum JL, Barr MM (2006). General and cell-type specific mechanisms target TRPP2/PKD-2 to cilia. Development 133, 3859–3870.

Barnes N, Tsivkovskii R, Tsivkovskaia N, Lutsenko S (2005). The copper-transporting ATPases, Menkes and Wilson disease proteins, have distinct roles in adult and developing cerebellum. J Biol Chem 280, 9640–9645.

Boehm M, Bonifacino JS (2001). Adaptins: the final recount. Mol Biol Cell 12, 2907–2920.

Bonifacino JS (2014). Adaptor proteins involved in polarized sorting. J Cell Biol 204, 7–17.

Bonnemaison M, Back N, Lin Y, Bonifacino JS, Mains R, Eipper B (2014). AP-1a controls secretory granule biogenesis and trafficking of membrane secretory granule proteins. Traffic 15, 1099–1121.

Braiterman L, Nyasae L, Leves F, Hubbard AL (2011). Critical roles for the COOH terminus of the Cu-ATPase ATP7B in protein stability, trans-Golgi network retention, copper sensing, and retrograde trafficking. Am J Physiol Gastrointest Liver Physiol 301, G69–G81.

Carvajal-Gonzalez JM, Gravotta D, Mattera R, Diaz F, Perez Bay A, Roman AC, Schreiner RP, Thuenauer R, Bonifacino JS, Rodriguez-Boulan E (2012). Basolateral sorting of the coxsackie and adenovirus receptor through interaction of a canonical YXXPhi motif with the clathrin adaptors AP-1A and AP-1B. Proc Natl Acad Sci USA 109, 3820–3825.

Cater MA, La Fontaine S, Shield K, Deal Y, Mercer JF (2006). ATP7B mediates vesicular sequestration of copper: insight into biliary copper excretion. Gastroenterology 130, 493–506.

Dell'Angelica EC, Klumperman J, Stoorvogel W, Bonifacino JS (1998). Association of the AP-3 adaptor complex with clathrin. Science 280, 431–434.

Doray B, Lee I, Knisely J, Bu G, Kornfeld S (2007). The gamma/sigma1 and alpha/sigma2 hemicomplexes of clathrin adaptors AP-1 and AP-2 harbor the dileucine recognition site. Mol Biol Cell 18, 1887–1896.

Dwyer ND, Adler CE, Crump JG, L'Etoile ND, Bargmann CI (2001). Polarized dendritic transport and the AP-1 mu1 clathrin adaptor UNC-101 localize odorant receptors to olfactory cilia. Neuron 31, 277–287.

Emre S, Atillasoy EO, Ozdemir S, Schilsky M, Rathna Varma CV, Thung SN, Sternlieb I, Guy SR, Sheiner PA, Schwartz ME, Miller CM (2001). Orthotopic liver transplantation for Wilson's disease: a single-center experience. Transplantation 72, 1232–1236.

Farias GG, Cuitino L, Guo X, Ren X, Jarnik M, Mattera R, Bonifacino JS (2012). Signal-mediated, AP-1/clathrin-dependent sorting of transmembrane receptors to the somatodendritic domain of hippocampal neurons. Neuron 75, 810–823.

Folsch H, Ohno H, Bonifacino JS, Mellman I (1999). A novel clathrin adaptor complex mediates basolateral targeting in polarized epithelial cells. Cell 99, 189–198.

Francis MJ, Jones EE, Levy ER, Ponnambalam S, Chelly J, Monaco AP (1998). A Golgi localization signal identified in the Menkes recombinant protein. Hum Mol Genet 7, 1245–1252.

Gravotta D, Carvajal-Gonzalez JM, Mattera R, Deborde S, Banfelder JR, Bonifacino JS, Rodriguez-Boulan E (2012). The clathrin adaptor AP-1A mediates basolateral polarity. Dev Cell 22, 811–823.

Guo X, Mattera R, Ren X, Chen Y, Retamal C, Gonzalez A, Bonifacino JS (2013). The adaptor protein-1 mu1B subunit expands the repertoire of basolateral sorting signal recognition in epithelial cells. Dev Cell 27, 353–366.

Guo Y, Nyasae L, Braiterman LT, Hubbard AL (2005). NH2-terminal signals in ATP7B Cu-ATPase mediate its Cu-dependent anterograde traffic in polarized hepatic cells. Am J Physiol Gastrointest Liver Physiol 289, G904–G916.

Heldwein EE, Macia E, Wang J, Yin HL, Kirchhausen T, Harrison SC (2004). Crystal structure of the clathrin adaptor protein 1 core. Proc Natl Acad Sci USA 101, 14108–14113.

Hirst J, Borner GH, Antrobus R, Peden AA, Hodson NA, Sahlender DA, Robinson MS (2012). Distinct and overlapping roles for AP-1 and GGAs revealed by the "knocksideways" system. Curr Biol 22, 1711–1716.

Holloway ZG, Velayos-Baeza A, Howell GJ, Levecque C, Ponnambalam S, Sztul E, Monaco AP (2013). Trafficking of the Menkes copper transporter ATP7A is regulated by clathrin-, AP-2-, AP-1-, and Rab22-dependent steps. Mol Biol Cell 24, 1735–1748.

Humphrey JS, Peters PJ, Yuan LC, Bonifacino JS (1993). Localization of TGN38 to the trans-Golgi network: involvement of a cytoplasmic tyrosine-containing sequence. J Cell Biol 120, 1123–1135.

Hung IH, Suzuki M, Yamaguchi Y, Yuan DS, Klausner RD, Gitlin JD (1997). Biochemical characterization of the Wilson disease protein and functional expression in the yeast Saccharomyces cerevisiae. J Biol Chem 272, 21461–21466.

Janvier K, Kato Y, Boehm M, Rose JR, Martina JA, Kim BY, Venkatesan S, Bonifacino JS (2003). Recognition of dileucine-based sorting signals from HIV-1 Nef and LIMP-II by the AP-1 gamma-sigma1 and AP-3 delta-sigma3 hemicomplexes. J Cell Biol 163, 1281–1290.

Jareb M, Banker G (1998). The polarized sorting of membrane proteins expressed in cultured hippocampal neurons using viral vectors. Neuron 20, 855–867.

Kaech S, Banker G (2006). Culturing hippocampal neurons. Nat Protoc 1, 2406–2415.

Kaler SG (2013). Inborn errors of copper metabolism. Handb Clin Neurol 113, 1745–1754.

Kelly BT, McCoy AJ, Spate K, Miller SE, Evans PR, Honing S, Owen DJ (2008). A structural explanation for the binding of endocytic dileucine motifs by the AP2 complex. Nature 456, 976–979.

Kennerson ML, Nicholson GA, Kaler SG, Kowalski B, Mercer JF, Tang J, Llanos RM, Chu S, Takata RI, Speck-Martins CE, *et al.* (2010). Missense mutations in the copper transporter gene ATP7A cause X-linked distal hereditary motor neuropathy. Am J Hum Genet 86, 343–352.

Kuo YM, Gitschier J, Packman S (1997). Developmental expression of the mouse mottled and toxic milk genes suggests distinct functions for the Menkes and Wilson disease copper transporters. Hum Mol Genet 6, 1043–1049.

La Fontaine S, Firth SD, Lockhart PJ, Brooks H, Parton RG, Camakaris J, Mercer JF (1998). Functional analysis and intracellular localization of the human menkes protein (MNK) stably expressed from a cDNA construct in Chinese hamster ovary cells (CHO-K1). Hum Mol Genet 7, 1293–1300.

Lalioti V, Hernandez-Tiedra S, Sandoval IV (2014). DKWSLLL, a versatile DXXXLL-type signal with distinct roles in the Cu -regulated trafficking of ATP7B. Traffic. 8, 839–860.

Lasiecka ZM, Winckler B (2011). Mechanisms of polarized membrane trafficking in neurons—focusing in on endosomes. Mol Cell Neurosci 48, 278–287.

Margeta MA, Wang GJ, Shen K (2009). Clathrin adaptor AP-1 complex excludes multiple postsynaptic receptors from axons in C. elegans. Proc Natl Acad Sci USA 106, 1632–1637.

Mar FM, Simoes AR, Leite S, Morgado MM, Santos TE, Rodrigo IS, Teixeira CA, Misgeld T, Sousa MM (2014). CNS axons globally increase axonal transport after peripheral conditioning. J Neurosci 34, 5965–5970.

Martinelli D, Travaglini L, Drouin CA, Ceballos-Picot I, Rizza T, Bertini E, Carrozzo R, Petrini S, de Lonlay P, El Hachem M, *et al.* (2013).

MEDNIK syndrome: a novel defect of copper metabolism treatable by zinc acetate therapy. Brain 136, 872–881.
Mattera R, Boehm M, Chaudhuri R, Prabhu Y, Bonifacino JS (2011). Conservation and diversification of dileucine signal recognition by adaptor protein (AP) complex variants. J Biol Chem 286, 2022–2030.
Mattera R, Farias GG, Mardones GA, Bonifacino JS (2014). Co-assembly of viral envelope glycoproteins regulates their polarized sorting in neurons. PLoS Pathog 10, e1004107.
Montpetit A, Cote S, Brustein E, Drouin CA, Lapointe L, Boudreau M, Meloche C, Drouin R, Hudson TJ, Drapeau P, Cossette P (2008). Disruption of AP1S1, causing a novel neurocutaneous syndrome, perturbs development of the skin and spinal cord. PLoS Genet 4, e1000296.
Ohno H, Stewart J, Fournier MC, Bosshart H, Rhee I, Miyatake S, Saito T, Gallusser A, Kirchhausen T, Bonifacino JS (1995). Interaction of tyrosine-based sorting signals with clathrin-associated proteins. Science 269, 1872–1875.
Otero MG, Alloatti M, Cromberg LE, Almenar-Queralt A, Encalada SE, Pozo Devoto VM, Bruno L, Goldstein LS, Falzone TL (2014). Fast axonal transport of the proteasome complex depends on membrane interaction and molecular motor function. J Cell Sci 127, 1537–1549.
Peden AA, Park GY, Scheller RH (2001). The di-leucine motif of vesicle-associated membrane protein 4 is required for its localization and AP-1 binding. J Biol Chem 276, 49183–49187.
Petris MJ, Camakaris J, Greenough M, LaFontaine S, Mercer JF (1998). A C-terminal di-leucine is required for localization of the Menkes protein in the trans-Golgi network. Hum Mol Genet 7, 2063–2071.
Petris MJ, Mercer JF, Culvenor JG, Lockhart P, Gleeson PA, Camakaris J (1996). Ligand-regulated transport of the Menkes copper P-type ATPase efflux pump from the Golgi apparatus to the plasma membrane: a novel mechanism of regulated trafficking. EMBO J 15, 6084–6095.
Polishchuk EV, Concilli M, Iacobacci S, Chesi G, Pastore N, Piccolo P, Paladino S, Baldantoni D, van IJzendoorn SC, Chan J, *et al.* (2014). Wilson disease protein ATP7B utilizes lysosomal exocytosis to maintain copper homeostasis. Dev Cell 29, 686–700.
Polishchuk R, Lutsenko S (2013). Golgi in copper homeostasis: a view from the membrane trafficking field. Histochem Cell Biol 140, 285–295.
Poyatos I, Ruberti F, Martinez-Maza R, Gimenez C, Dotti CG, Zafra F (2000). Polarized distribution of glycine transporter isoforms in epithelial and neuronal cells. Mol Cell Neurosci 15, 99–111.
Ren X, Farias GG, Canagarajah BJ, Bonifacino JS, Hurley JH (2013). Structural basis for recruitment and activation of the AP-1 clathrin adaptor complex by Arf1. Cell 152, 755–767.
Ren X, Park SY, Bonifacino JS, Hurley JH (2014). How HIV-1 Nef hijacks the AP-2 clathrin adaptor to downregulate CD4. Elife 3, e01754.
Rivera JF, Ahmad S, Quick MW, Liman ER, Arnold DB (2003). An evolutionarily conserved dileucine motif in Shal K+ channels mediates dendritic targeting. Nat Neurosci 6, 243–250.
Robinson MS (2004). Adaptable adaptors for coated vesicles. Trends Cell Biol 14, 167–174.
Roelofsen H, Wolters H, Van Luyn MJ, Miura N, Kuipers F, Vonk RJ (2000). Copper-induced apical trafficking of ATP7B in polarized hepatoma cells provides a mechanism for biliary copper excretion. Gastroenterology 119, 782–793.
Saito T, Okabe M, Hosokawa T, Kurasaki M, Hata A, Endo F, Nagano K, Matsuda I, Urakami K, Saito K (1999). Immunohistochemical determination of the Wilson Copper-transporting P-type ATPase in the brain tissues of the rat. Neurosci Lett 266, 13–16.
Schumacher G, Platz KP, Mueller AR, Neuhaus R, Luck W, Langrehr JM, Settmacher U, Steinmueller T, Becker M, Neuhaus P (2001). Liver transplantation in neurologic Wilson's disease. Transplant Proc 33, 1518–1519.
Tran TH, Zeng Q, Hong W (2007). VAMP4 cycles from the cell surface to the trans-Golgi network via sorting and recycling endosomes. J Cell Sci 120, 1028–1041.
Traub LM, Bonifacino JS (2013). Cargo recognition in clathrin-mediated endocytosis. Cold Spring Harb Perspect Biol 5, a016790.
Wang Y, Hodgkinson V, Zhu S, Weisman GA, Petris MJ (2011). Advances in the understanding of mammalian copper transporters. Adv Nutr 2, 129–137.
West AE, Neve RL, Buckley KM (1997). Targeting of the synaptic vesicle protein synaptobrevin in the axon of cultured hippocampal neurons: evidence for two distinct sorting steps. J Cell Biol 139, 917–927.
Yamaguchi Y, Heiny ME, Suzuki M, Gitlin JD (1996). Biochemical characterization and intracellular localization of the Menkes disease protein. Proc Natl Acad Sci USA 93, 14030–14035.
Yi L, Donsante A, Kennerson ML, Mercer JF, Garbern JY, Kaler SG (2012). Altered intracellular localization and valosin-containing protein (p97 VCP) interaction underlie ATP7A-related distal motor neuropathy. Hum Mol Genet 21, 1794–1807.